Atmos. Chem. Phys., 7, 5599–5610, 2007
www.atmos-chem-phys.net/7/5599/2007/

Atmospheric Chemistry and Physics

The SOA/VOC/NO_x system: an explicit model of secondary organic aerosol formation

M. Camredon[1], B. Aumont[1], J. Lee-Taylor[2], and S. Madronich[2]

[1]Laboratoire Interuniversitaire des Systèmes Atmosphériques, UMR CNRS 7583, Universités Paris 7 et Paris 12, 94010 Créteil Cedex, France
[2]National Center for Atmospheric Research, Atmospheric Chemistry Division, P.O. Box 3000, Boulder, Colorado 80307, USA

Received: 11 June 2007 – Published in Atmos. Chem. Phys. Discuss.: 2 August 2007
Revised: 12 October 2007 – Accepted: 29 October 2007 – Published: 13 November 2007

Abstract. Our current understanding of secondary organic aerosol (SOA) formation is limited by our knowledge of gaseous secondary organics involved in gas/particle partitioning. The objective of this study is to explore (i) the potential for products of multiple oxidation steps contributing to SOA, and (ii) the evolution of the SOA/VOC/NO_x system. We developed an explicit model based on the coupling of detailed gas-phase oxidation schemes with a thermodynamic condensation module. Such a model allows prediction of SOA mass and speciation on the basis of first principles. The SOA/VOC/NO_x system is studied for the oxidation of 1-octene under atmospherically relevant concentrations. In this study, gaseous oxidation of octene is simulated to lead to SOA formation. Contributors to SOA formation are shown to be formed via multiple oxidation steps of the parent hydrocarbon. The behaviour of the SOA/VOC/NO_x system simulated using the explicit model agrees with general tendencies observed during laboratory chamber experiments. This explicit modelling of SOA formation appears as a useful exploratory tool to (i) support interpretations of SOA formation observed in laboratory chamber experiments, (ii) give some insights on SOA formation under atmospherically relevant conditions and (iii) investigate implications for the regional/global lifetimes of the SOA.

1 Introduction

Progressive gas-phase oxidation of volatile organic compounds (VOC) leads to the formation of a multitude of intermediate species (e.g., Aumont et al., 2005). These secondary organics are more functionalised than their precursor compounds, and the number of functions typically increases as oxidation proceeds. Highly functionalised species typically have lower saturation vapour pressures and/or higher polarities, allowing substantial gas/particle partitioning, thus leading to secondary organic aerosol (SOA) formation. Once in the aerosol phase, those compounds react further by photochemical reactions that alter particulate composition (e.g., Molina et al., 2004; Stephanou, 2005). Recent measurements indicate that SOA products can react via heterogeneous or particle-phase reactions, forming oligomeric and/or polymeric species, responsible for an important fraction of SOA growth (e.g., Jang et al., 2002; Gao et al., 2004; Kalberer et al., 2004; Tolocka et al., 2004).

Despite the substantial impacts of SOA on the environment, SOA modelling is not satisfactorily constrained. A large underestimation of SOA production in current models has been highlighted by recent observations in the boundary layer (e.g., de Gouw et al., 2005; Johnson et al., 2006; Volkamer et al., 2006) as well as in the free troposphere (Heald et al., 2005). Our current understanding of SOA formation is limited by the lack of knowledge of gaseous secondary organics involved in gas/particle partitioning. SOA formation involves a multitude of semi-volatile organic compounds (SVOC) having complex molecular structures. Their low atmospheric concentrations cause analytical difficulties (e.g., Jacobson et al., 2000; Turpin et al., 2000; Kanakidou et al., 2005). During in situ measurement campaigns, less than 20% of the total particulate organic mass is typically identified (Rogge et al., 1993; Puxbaum et al., 2000). Moreover major difficulties hinder the simulation of SOA formation on the basis of first principles. Most three-dimensional transport models were developed to represent the chemical evolution

Correspondence to: B. Aumont
(aumont@lisa.univ-paris12.fr)

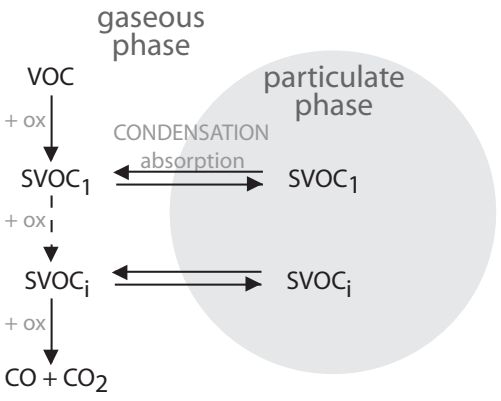

Fig. 1. Schematic diagram of the explicit model of SOA formation.

of the O_3/VOC/NO_x system. These models typically represent organic chemistry with highly simplified mechanisms using lumped or surrogate species (e.g., Gery et al., 1989; Stockwell et al., 1997; Bey et al., 2001; Brasseur et al., 1998; Carter, 2000; Poisson et al., 2000). The formation of long chain functionalised secondary organics acting as SOA precursors is ignored in those gas-phase oxidation schemes.

Parameterized SOA representations are therefore implemented in 3-D chemistry-transport models in terms of total particle growth. The aerosol creation potential measured in laboratory chamber experiments from a particular hydrocarbon, HC, is currently expressed in terms of aerosol yield Y defined as:

$$Y = \frac{M_o}{\Delta[\mathrm{HC}]} \quad (1)$$

where M_o is the organic aerosol mass concentration produced for a given amount of HC reacted (Δ[HC]). The aerosol yield strongly depends on the organic particulate mass which acts as the medium into which oxidation products can be absorbed (e.g., Odum et al., 1996, 1997). Odum et al. (1996) demonstrated that the evolution of aerosol yield with M_o can be expressed as:

$$Y = M_o \sum \left(\frac{\alpha_i K_{om,i}}{1 + K_{om,i} M_o} \right) \quad (2)$$

where α_i is the mass stoichiometric factor of the aerosol-forming species i and $K_{om,i}$ is the equilibrium partitioning coefficient for species i. Odum et al. (1996, 1997) showed that the use of two lumped aerosol-forming products for Eq. (2) fits laboratory yield data with sufficient accuracy. Equation (2) is considered valid only for the final aerosol yield. This semi-empirical two-product model has been extensively used in 3-D chemistry-transport models (e.g., Hoffman et al., 1997; Kanakidou et al., 2000; Schell et al., 2001; Chung and Seinfeld, 2002; Tsigaridis and Kanakidou, 2003) where constants α_i and $K_{om,i}$ are chosen as the best fit of laboratory chamber data for a given HC.

However, the two-product representation assumes that aerosol-forming species i is produced from a single oxidation step of the parent hydrocarbon. SVOC formation is suspected to be more complex than arising from first generation oxidation products of a given precursor, with the possibility of multiple oxidation steps (Kroll and Seinfeld, 2005; Ng et al., 2006, 2007). The relative importance as contributors to SOA formation of those products formed from multiple oxidation steps with regard to direct oxidation products of the parent hydrocarbon remains unknown (e.g., Kroll and Seinfeld, 2005).

Furthermore, this empirical representation for SOA formation implies a large extrapolation of experimental chamber results carried out at levels of NO_x and HC that are significantly higher than typical tropospheric conditions (e.g., Cocker et al., 2001; Vesterinen et al., 2007; Kroll et al., 2007). The potential of an air mass to attain supersaturation during its ageing depends on local chemical factors, especially (i) the emitted HC source amounts influencing the concentration of secondary organic carbon in the plume and (ii) NO_x chemical regimes that drive the chemical identity of SVOC produced during air mass oxidation (i.e. carbon atom number, nature and distribution of functional groups borne by the molecule...), and consequently their volatility. The evolution of the SOA/VOC/NO_x system still remains difficult to ascertain.

The objective of this work is to explore (i) the role of products of multiple oxidation steps in the production of SOA contributors and (ii) the evolution of the SOA/VOC/NO_x system. For this purpose, we developed an explicit model describing SOA formation based on thermodynamic and chemical principles that predicts the gas/particle partitioning of individual organics produced during gas-phase oxidation. Such a model allows therefore prediction of SOA mass and speciation on the basis of first-principles. The model is based on the coupling of explicit gas-phase oxidation schemes with a thermodynamic module for condensation (see Fig. 1). Gas-phase oxidation schemes up to CO_2 production are developed using the explicit self-generating approach described by Aumont et al. (2005). Gas/particle partitioning of low-volatility species is represented assuming (i) a basic thermodynamic absorption process (e.g., Pankow, 1994a) and (ii) that the aerosol phase behaves as a pure ideal organic phase. In this exploratory study, no reactions are implemented in the particulate phase. SOA formation is studied here for the complete oxidation of 1-octene. This work has been carried out with a particular focus on the gas/aerosol carbon budget. Section 2 describes the explicit model for SOA formation. The scenarios selected to explore the SOA/VOC/NO_x system are presented in Sect. 3. SOA formation from multiple oxidation steps of the parent HC is reported in Sect. 4. The simulated evolution of the SOA/VOC/NO_x system is discussed in Sect. 5.

2 SOA formation model

SVOC production might require many successive oxidation steps. Most reaction pathways involved during gas-phase oxidation make minor individual contributions to the organic budget. These minor reaction channels are therefore ignored in current mechanisms, even in the most detailed mechanisms available to date such as the NCAR Master Mechanism (Madronich and Calvert, 1990; Aumont et al., 2000) or the University of Leeds' Master Chemical Mechanism (MCM-v3) (Jenkin et al., 2003; Saunders et al., 2003). However, these minor pathways could have a cumulative importance for the formation of those low-volatility species. Highly detailed oxidation schemes are therefore required to simulate the behaviour of organic species during gas-phase oxidation and their interaction with the organic aerosol phase. Such explicit schemes involve a very large number of chemical reactions and intermediate species, far in excess of the number that can be reasonably written manually (Aumont et al., 2005).

2.1 Gas-phase oxidation schemes

Explicit gas-phase oxidation schemes are written using the self-generating approach developed by Aumont et al. (2005). This expert system is based on two main elements:

1. A protocol defining a set of rules that lay out the choice of reaction pathways and provide the rate coefficients needed in the mechanism. When available, kinetic data taken from laboratory measurements are assigned to the chemical scheme. Otherwise, an estimation of the rate constant, stoichiometric coefficients and reaction products is performed using structure/activity relationships.

2. A generator which is a computer program that automatically creates the fully-explicit degradation scheme, up to CO and CO_2, for a set of parent species provided as input on the basis of the predefined protocol.

The protocol and the main running stages of the generator are described in detail by Aumont et al. (2005). Only salient points are summarized here. The development of self-generated chemical schemes requires the identification of all the reactions for each emitted organic compound and for their reaction products. These reactions generally include: (i) initiation of atmospheric degradation by attack with OH, NO_3, O_3 or photolysis, leading to the formation of peroxy radicals, (ii) reactions of peroxy radicals with NO, NO_2, NO_3, HO_2 and with other RO_2 radicals leading to the formation of stable reaction intermediates or alkoxy radicals RO and (iii) alkoxy radical reactions with O_2, unimolecular decomposition or isomerisation leading to the formation of stable reaction intermediates or new peroxy radicals. The possible functional groups produced during the oxidation of parent compounds are ketones, aldehydes, alcohols, hydroperoxides, nitrates, peroxy radicals, alkoxy radicals, carboxylic acids, peracids, peroxyacylnitrates and peroxyacyl radicals. The total number of species generated to fully describe the oxidation grows exponentially with increasing carbon number of precursor (Aumont et al., 2005).

2.2 Gas/particle partitioning of semi-volatile organic compounds

The dominant process controlling the gas/particle partitioning of SVOC is expected to be an absorption mechanism (Pankow, 1994a,b; Odum et al., 1996; Hoffman et al., 1997; Griffin et al., 1999; Kalberer et al., 2000). The gas/particle partitioning of organics produced during the gas-phase degradation is based on the absorptive model described by Pankow (1994a,b), which assumes a thermodynamic equilibrium of gaseous oxidation products between gas and particulate phases. Gas/particle partitioning of each organic species can then be described on the basis of Raoult's law:

$$P_i = x_i \gamma_i P_i^{\mathrm{vap}} \tag{3}$$

where P_i is the equilibrium partial pressure of a species i, x_i its mole fraction in the aerosol phase, P_i^{vap} its vapour pressure as pure liquid at the temperature of interest and γ_i its activity coefficient in the aerosol phase. Only equilibria for non-radical intermediate species are considered here.

For aerosol particles expected to be composed of a mixture of similar-type molecules, γ_i is set to unity (e.g., Seinfeld and Pankow, 2003). The liquid vapour pressure (subcooled if necessary) of organic species is estimated using the Myrdal and Yalkowsky method (Myrdal and Yalkowsky, 1997), owing to its reliability for SVOC generated during tropospheric gas-phase oxidation (Camredon and Aumont, 2006). The Myrdal and Yalkowsky method is coupled with the Joback structure/property relationship for boiling point estimates (e.g., Reid et al., 1986). Additional group contributions are included to evaluate the vapour pressure of the wide range of compounds involved in SOA formation (see Camredon and Aumont, 2006).

In this exploratory study, no reactions are implemented in the particulate phase. Heterogeneous reactions would shift condensation equilibria towards the aerosol phase. As long as the products of any heterogeneous reactions were less volatile than their reactants, such processes would lead to additional mass in the condensed phase. The aerosol mass simulated here can therefore be seen as a lower limit (e.g., Kroll and Seinfeld, 2005).

2.3 System resolution

Time integration for chemical schemes is performed using the two-step solver (Verwer, 1994; Verwer et al., 1996). The gas-phase lifetimes of SVOC are typically greater than half an hour. The characteristic time associated with the gas/particle mass transfer is assumed to be short compared

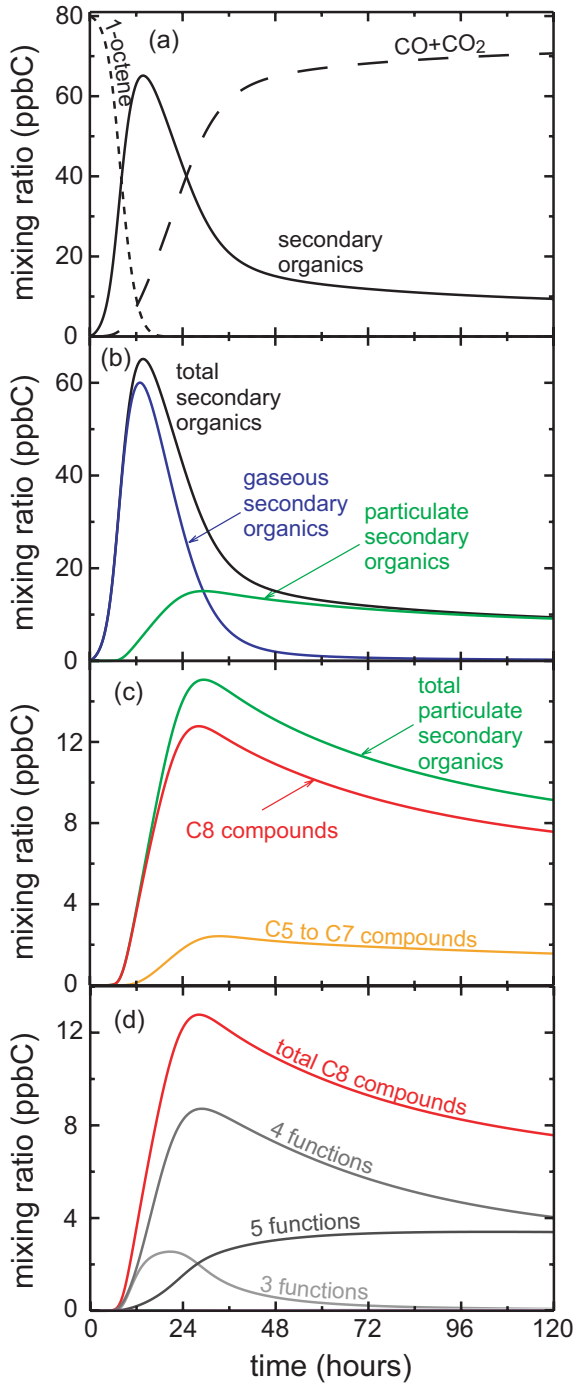

Fig. 2. Time evolution of carbonaceous species in the particulate phase during the simulation carried out under 1 ppb of NO_x and starting with an initial loading of 10 ppb of 1-octene. Panel **(a)**: distribution of the carbon. Panel **(b)**: distribution of secondary organics. Panel **(c)**: distribution of particulate organics as a function of carbon chain length. Panel **(d)**: distribution of particulate C8 organics as a function of the number of functional groups borne by the molecules.

to the timescale required for other production/removal processes of gaseous SVOC. Hence, thermodynamic equilibrium was imposed at each time step (20 min). Gas/particle equilibrium is solved using the iterative method described by Pankow (1994b). For the case of 1-octene presented below, the number of species considered to describe gas-phase oxidation is about 1.4×10^6. Thermodynamic equilibrium is considered for about 4.0×10^5 of these oxidation products. To our knowledge, this is the first attempt to describe SOA formation on the basis of a fully explicit model.

3 Scenarios

The SOA/VOC/NO_x system is studied here for the complete oxidation of 1-octene. This species was selected as a representative parent compound because (i) the aerosol creation potential of 1-octene has been reported experimentally (Wang et al., 1992; Forstner et al., 1997), (ii) the first steps in gaseous oxidation of alkenes are relatively well established (e.g., Calvert et al., 2000) and (iii) SOA formation is expected from multiple oxidation steps of this volatile precursor.

The aerosol creation potential of 1-octene is simulated in a box model. Physical conditions and chemical regimes are held constant throughout the simulation in order to isolate the influence of the initial hydrocarbon concentration or NO_x regimes on SOA formation. Relative humidity is set to 50%. Temperature is fixed at 298 K. Photolysis frequencies are computed for a zenith angle of 30 degrees for mid-latitude conditions using the TUV model (Madronich and Flocke, 1998). Simulations are performed under various fixed NO_x mixing ratios, between 50 ppt and 100 ppb. NO_x levels are adjusted at each time step to sustain the prescribed NO_x mixing ratio. Finally, simulations are carried out for various initial mixing ratios of the parent hydrocarbon, $[HC]_0$, ranging from 1 to 100 ppb.

4 Typical temporal evolution of SOA mass and speciation

Results are presented here with a particular focus on the gradual change of organic compounds in the particulate phase during gas-phase oxidation. The various simulations present similar characteristics. Typical profiles are illustrated with results obtained for the simulation carried out under 1 ppb of NO_x and starting with an initial loading of 10 ppb of octene. Under those conditions, octene removal is dominated by OH radical chemistry (with a reactivity yield toward OH higher than 90%).

The temporal evolutions of octene, secondary organics and inorganic carbon (i.e. $CO+CO_2$) during the simulation are shown in Fig. 2a. For the conditions simulated here, the precursor is essentially consumed after 20 h of irradiation. At this time, secondary organics represent the major fraction of

the carbon. This fraction is then progressively oxidised in the gas-phase into CO and CO_2.

The distribution of secondary organics between the gaseous and particulate phases is shown in Fig. 2b. SOA mass only appears when a significant fraction (50%) of precursor has been oxidised. Aerosol mass reaches a maximum after about 30 h of oxidation and a slight decrease of SOA mass is then observed. As no aerosol phase reactions are implemented in the model, the gas/particle equilibria of the more volatile compounds are progressively shifted from particle to gas, as gas-phase oxidation proceeds. Once in the gaseous phase, those compounds evolve by oxidation until the final formation of CO and CO_2. A significant fraction of the carbon still remains in the condensed phase (about 15% of the carbon at the end of the simulation).

The distribution of particulate organics is shown as a function of the chain length in Fig. 2c. This fraction is dominated by species holding 8 carbon atoms, i.e. of the same size as the parent compound. As oxidation proceeds and particulate mass increases, the amount of compounds with shorter carbon chain length also increases.

The distribution of particulate organic compounds bearing 8 carbons is shown in Fig. 2d as a function of the number of functional groups borne by the molecules. C8 compounds in the condensed phase mainly bear 4 functional groups. After 30 h of oxidation, those compounds volatilise into the gas phase again. Tri-functionalised C8 compounds are found in the aerosol phase at the beginning of the oxidation but volatilise rapidly back to the gas phase after 24 h. Species bearing 5 functions appear in particulate matter as gas-phase oxidation proceeds and for the conditions simulated here remain in the particle phase.

The distribution of the organic moieties in the particulate phase is shown as a function of time in Fig. 3. Results are expressed as an organic functional group (OF_k) per particulate carbon ratio as:

$$R_{OFk/\mathrm{C}} = \frac{\sum_i n_i^{OFk} C_i}{\sum_i n_i^{C} C_i} \quad (4)$$

where C_i is the concentration of molecule i in the aerosol phase and $n_i^{OF_k}$ or n_i^C are the number of organic functions k or carbon atoms in the molecule i, respectively. The substitution degree of the carbon (i.e. $\sum_k R_{OFk/\mathrm{C}}$) is found to be slightly sensitive to oxidation time. As expected, the degree of substitution is rather high with values of about 50%. The dominant moieties in the particulate phase are found to be the alcohol ($R_{-\mathrm{OH}/\mathrm{C}}$=18%), nitrate ($R_{-\mathrm{ONO_2}/\mathrm{C}}$=18%) and ketone ($R_{-\mathrm{CO}-/\mathrm{C}}$=13%) moieties. Hydroperoxides and PANs are found in the 3% range.

In this exploratory study, gaseous oxidation of a relatively high-volatility hydrocarbon, 1-octene, is simulated to lead to SOA formation for representative concentrations of tropospheric levels. Contributors to SOA formation are shown

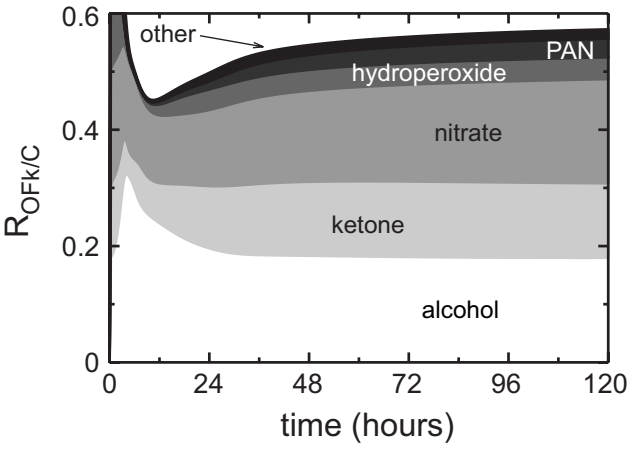

Fig. 3. Time evolution of the organic functional group per particulate carbon ratio ($R_{OFk/\mathrm{C}}$) during the simulation carried out under 1 ppb of NO_x and starting with an initial loading of 10 ppb of 1-octene.

to be highly functionalised products, bearing at least 3 functional groups. These compounds are formed via multiple oxidation steps of the parent HC. Time scales of a few days are indeed required to form those low vapour pressure products. This delay may explain why negligible or small SOA formation is observed in laboratory chamber experiments from the oxidation of relatively high-volatility precursors. Comparisons of simulated SOA mass with in situ observations highlight a systematic underestimation of SOA production (Volkamer et al., 2006). Volkamer et al. (2006) showed that these discrepancies increase with the ageing of air masses. We show here that volatile precursors might lead to SOA formation after multiple oxidation steps. Such processes are currently ignored in models and may explain the gap between observed and simulated SOA concentrations. Furthermore, some SOA contributors (especially the 4- and 5-functional C8 species) have very low vapour pressure. These compounds remain preferentially in the aerosol phase and SOA evaporation is a slow process. Therefore lifetime of SOA appears likely driven by aerosol reactivity and/or microphysical processes.

5 The SOA/VOC/NO_x system

The formation of SOA has been illustrated in the previous section with a simulation carried out under 1 ppb of NO_x and starting with an initial loading of 10 ppb of octene. SOA formation is quite sensitive to external parameters such as the initial mixing ratio of the parent hydrocarbon, $[HC]_0$, and NO_x-levels. The sensitivity of the SOA/VOC/NO_x system is explored here with a particular focus on (i) the maximum aerosol yield, (ii) the temporal evolution of SOA formation and (iii) SOA speciation. The objective of this section is

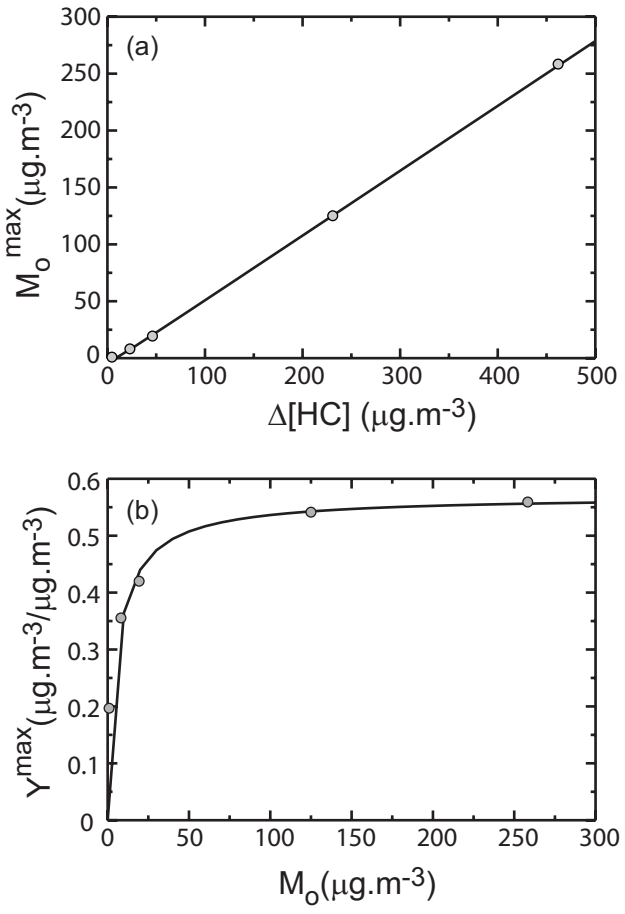

Fig. 4. Final growth curve **(a)** and final yield curve **(b)** simulated for the oxidation of 1-octene under 1 ppb of NO_x. Five simulations were carried out with various initial loads of 1-octene. Each circle represents $Y^{\max}$ or $M_o^{\max}$ obtained for a single simulation. The continuous line represents the fit of the simulated data from the two-product model (α_1=0.17, $K_{1,om}$=0.08, α_2=0.40, $K_{2,om}$=0.26).

to assess whether the behaviour simulated using the explicit modelling agrees with general tendencies observed during laboratory chamber experiments.

5.1 Maximum aerosol yields

5.1.1 Influence of $[HC]_0$

The dependence of SOA formation on the initial mixing ratio of the parent hydrocarbon has been widely studied in laboratory chamber experiments (e.g., Hurley et al., 2001; Song et al., 2005; Ng et al., 2006; Kroll et al., 2006). An increase of $[HC]_0$ leads directly to an increase of the aerosol organic mass, M_o, by increasing the concentrations of the SVOC in the system. An additional effect arises from the increase of the organic mass which acts as the medium into which oxidation product can be absorbed. The dependence of SOA formation on M_o is generally discussed by observing the evolution of the aerosol yield, Y, versus M_o (e.g., Odum et al., 1996, 1997; Song et al., 2005; Presto et al., 2005; Ng et al., 2007; Kroll et al., 2007). Y increases with M_o. Notable limit behaviours are that:

– At low particulate organic mass, Y strongly depends on M_o. For M_o equal to zero, a compound will partition into the particulate phase only if its concentration exceeds its saturation vapour pressure. When increasing M_o, products might be absorbed into the particle phase even though they are present at concentrations below their saturation point. The two-product model (see Eq. 2) predicts an aerosol yield that is directly proportional to M_o ($Y \rightarrow M_o \sum \alpha_i K_{om,i}$) when M_o tends to zero.

– At high particulate organic mass, Y is weakly dependent on M_o. The two-product model (see Eq. 2) predicts an aerosol yield that is independent of M_o ($Y \rightarrow \sum \alpha_i$) when M_o tends to infinity.

Figure 4 shows simulated evolutions of SOA formation as classical plots reported from laboratory chamber experiments: (a) the maximum aerosol mass (denoted $M_o^{\max}$ hereafter) as a function of Δ[HC] (the final growth plot as defined by Ng et al. (2006)) and (b) the maximum aerosol yield (denoted $Y^{\max}$ hereafter) as a function of organic aerosol mass concentration (the final yield plot as defined by Ng et al. (2006)). These plots are reported for simulations carried out under 10 ppb of NO_x. The set includes five $[HC]_0$ values: 1, 5, 10, 50 and 100 ppb. The final growth plot is of similar shape to those reported from laboratory chamber experiments (e.g., Hurley et al., 2001; Song et al., 2005; Ng et al., 2006; Kroll et al., 2006). $M_o^{\max}$ varies from about 3 to 250 $\mu g\,m^{-3}$ for 1 and 100 ppb of $[HC]_0$, respectively. The final yield plot also has the same shape as those observed in laboratory chamber experiments (e.g., Odum et al., 1996, 1997; Song et al., 2005; Presto et al., 2005; Ng et al., 2007; Kroll et al., 2007). $Y^{\max}$ ranges from about 0.2 to an asymptotic value of about 0.57. As expected, the effect on $Y^{\max}$ of changes in M_o is clearly more pronounced at low M_o than at higher values. The simulated results can be fitted by a two-product model, in the same way as is done from laboratory chamber measurements (e.g., Odum et al., 1996; Griffin et al., 1999). The final growth and yield curves for the two-product model optimized from the simulated results are presented in Fig. 4a and b respectively.

The explicit approach captures the general qualitative behaviours observed during laboratory chamber experiments of the dependence of SOA formation with $[HC]_0$, tendencies that are also reported by the two-product (e.g., Odum et al., 1996) or the one-product approaches (Kroll and Seinfeld, 2005).

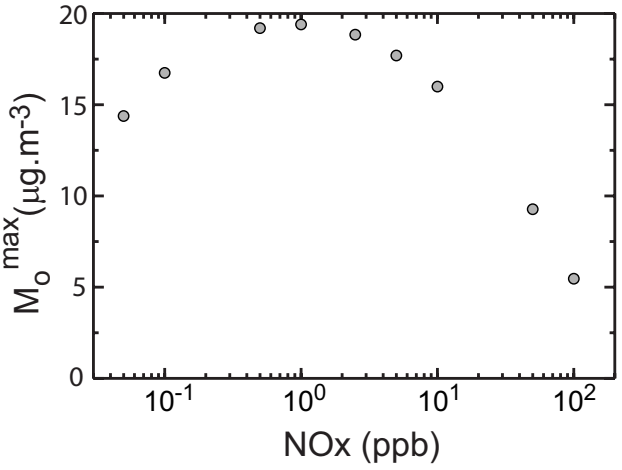

Fig. 5. M_o^{max} as a function of NO_x level simulated for the oxidation of an initial loading of 10 ppb of 1-octene. Nine simulations were carried out under various fixed NO_x levels. Each circle represents M_o^{max} obtained for a single simulation.

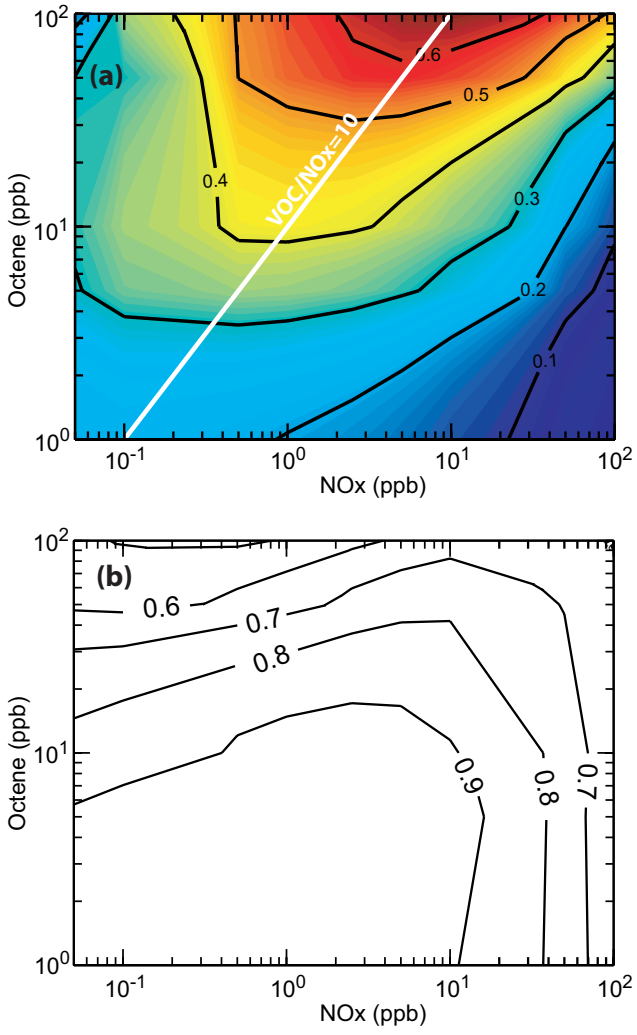

Fig. 6. Panel **(a)**: Y^{max} as a function of NO_x level and initial loading of 1-octene. The white continuous line is the constant [HC](ppb)/NO_x(ppb) ratio of 10. Panel **(b)**: Relative contribution of OH oxidation in the removal of 1-octene as a function of NO_x level and initial loading of 1-octene.

5.1.2 Influence of NO_x

NO_x-levels have been shown to largely influence SOA formation during laboratory chamber experiments. Conclusions of those experimental studies are that (i) a higher M_o is observed under low-NO_x experiments than under high-NO_x (e.g., Hatakeyama et al., 1991; Hurley et al., 2001; Johnson et al., 2004; Martin-Riviejo and Wirtz, 2005; Song et al., 2005; Presto et al., 2005; Ng et al., 2007; Kroll et al., 2007), (ii) at high NO_x, M_o is found to decrease with increasing NO_x (e.g., Pandis et al., 1991; Zhang et al., 1992; Kroll et al., 2006) and (iii) at low NO_x, M_o is found to increase with increasing NO_x (e.g., Pandis et al., 1991; Zhang et al., 1992; Kroll et al., 2006).

Figure 5 shows M_o^{max} as a function of NO_x level for simulations carried out with an initial loading of 10 ppb of $[HC]_0$. The set includes nine NO_x levels: 0.05, 0.1, 0.5, 1, 2.5, 5, 10, 50 and 100 ppb. Two regimes of SOA formation dependence on NO_x level are identified: a first regime, where M_o^{max} increases with NO_x and a second one, where M_o^{max} decreases when NO_x increases. Transition between those two regimes occurs at a NO_x mixing ratio of about 1 ppb. The simulated profile of M_o^{max} versus NO_x shows a similar shape to those reported from laboratory chamber experiments browsing NO_x levels from low to high NO_x (e.g., Kroll et al., 2006; Pandis et al., 1991; Zhang et al., 1992).

The explicit approach therefore captures the general features reported from laboratory chamber experiments of the influence of NO_x level on SOA formation. This explicit model can as a result be used as an exploratory tool to (i) facilitate interpretations of SOA formation observed in laboratory chamber experiments and (ii) give some insight into SOA formation under atmospherically relevant concentrations.

5.1.3 The SOA/VOC/NO_x system

The sensitivity of the SOA/VOC/NO_x system is explored here on the basis of 45 simulations, conducted with five different initial concentrations of octene (1, 5, 10, 50 and 100 ppb) under nine fixed NO_x concentrations (0.05, 0.1, 0.5, 1, 2.5, 5, 10, 50 and 100 ppb). Figure 6a shows Y^{max} as a function of NO_x level and initial loading of octene, as usually done for ozone isopleths.

At a fixed NO_x level, Y^{max} increases globally with increasing $[HC]_0$. As expected and discussed before, Y^{max} is found

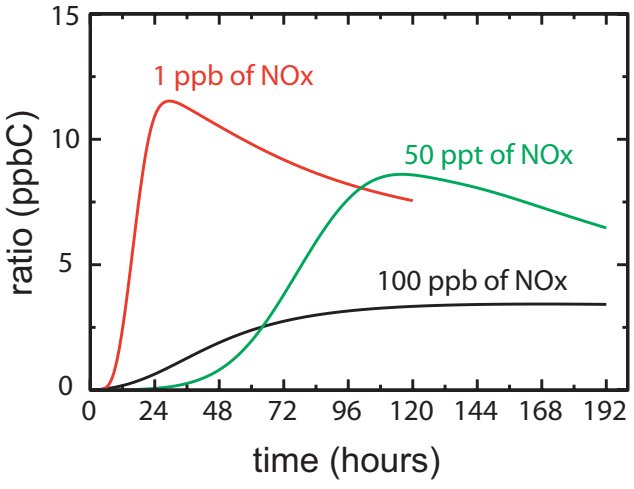

Fig. 7. Time evolution of secondary organics suspected to act as SOA contributors (i.e. C8 organics bearing at least 4 functional groups) summed across both phases for simulations starting with an initial loading of 10 ppb of 1-octene and carried out under 50 ppt, 1 ppb and 100 ppb of NO_x.

to be largely dependent on $[HC]_0$ at low $[HC]_0$. Y^{max} is expected to tend to an asymptotic value when $[HC]_0$ tends to infinity. This behaviour is observed at low NO_x levels but not at high NO_x. The simulated zone focuses on low $[HC]_0$, representative of atmospheric levels. The asymptotic value of Y^{max} is not reached under those conditions. At a fixed $[HC]_0$ value, two NO_x regimes are highlighted as specified before. Y^{max} increases with NO_x at low NO_x and shows an opposite behaviour at high NO_x. Note that Y^{max} is highly sensitive to NO_x at high $[HC]_0$, but remains weakly sensitive to NO_x at low $[HC]_0$. Maximum Y^{max} values are reached for an $[HC](ppb)/NO_x(ppb)$ ratio of about 10. This constant ratio is also reported in Fig. 6a. An increase or decrease of this ratio results in a decrease of simulated Y^{max}.

The limitation of SOA formation under high NO_x levels has been suggested to be the result of the change in (i) the relative level of oxidants, i.e. OH, O_3 and NO_3 (Hurley et al., 2001), and/or (ii) the branching ratio for the recombination of organo-peroxy radicals, RO_2 (e.g., Hatakeyama et al., 1991; Johnson et al., 2004; Presto et al., 2005; Kroll et al., 2006; Ng et al., 2007; Kroll et al., 2007). The increase of aerosol yields with increasing NO_x at low NO_x levels remains not understood (e.g., Kroll et al., 2006).

Gas/particle partitioning of a given SVOC occurs when its gas-phase concentration exceeds its equilibrium vapour pressure above a particle surface. Gas/particle partitioning of a given SVOC strongly depends on (i) its chemical identity defining its vapour pressure and (ii) its supersaturation state which is directly linked to its gas-phase concentration. According to the speciation of particulate organic matter given in Fig. 2d, SOA contributors are mainly C8 organic compounds bearing at least 4 functional groups. Figure 7 shows the time evolution of these secondary organics summed across both phases for simulations starting with an initial amount of 10 ppb of octene. Three cases are reported in Fig. 7 for various NO_x levels (50 ppt, 1 ppb and 100 ppb). For the low-NO_x case, the formation of secondary organic species is slow. A maximum concentration of about 8.5 ppbC is reached after 110 h. For the intermediate-NO_x case, the formation of secondary organics is fast and a maximum value of about 12 ppbC is reached after 30 h. Under high-NO_x conditions, the formation of secondary organic is slow and lower than for the low and intermediate NO_x levels. A maximum concentration of 3 ppbC is reached after 170 h. Formation and accumulation of multifunctional compounds bearing at least 4 functional groups is optimal for a NO_x level of a few ppb. This optimal condition of NO_x coincides with the maximum Y^{max} reached for an initial loading of 10 ppb of octene.

Various processes explain the evolution with NO_x level of secondary organics acting as SOA contributors. Figure 6b shows the relative contribution of OH oxidation in the removal of 1-octene as a function of NO_x level and initial loading of 1-octene. Under the simulated conditions, octene is mainly removed by OH radicals. NO_3 is responsible for less than 1% of octene oxidation. However reactivity toward O_3 can be significant, with an O_3 reaction yield reaching 50%. Reactions of 1-octene with O_3 break the $>C=C<$ bond and lead to the formation of smaller (and more volatile) compounds. Figures 6a and b show that for a given $[HC]_0$, the maximum Y^{max} is reached when the relative contribution of OH to the removal of the precursor is maximum. The dependence of SOA formation on NO_x can therefore be interpreted as being partially controlled by the differences in relative oxidant levels. In addition, under low and high NO_x, the oxidation rate is slow because of low oxidant concentrations. With a slow oxidation rate, the gas-phase concentration of secondary products increases slowly and the SVOC are consequently oxidised before they accumulate in particles (see Fig. 7). Furthermore under high NO_x levels, reactions with NO produce mostly alkoxy radicals, which can decompose to smaller (and more volatile) compounds. Simulated results lead to the conclusions that the dependence of Y^{max} with NO_x is here the result of (i) the relative contribution of gaseous oxidants, (ii) the gaseous oxidation rate and (iii) the gaseous radical chemistry.

5.2 Temporal behaviour

Ng et al. (2006) suggested that the shape of the time-dependent growth curve can give some insight into the processes involved in SOA formation. Especially, this shape reveals the importance and the relative contribution of second generation products to SOA growth.

Figure 8 reports the time-dependent growth curve for simulations carried out under 10 ppb of NO_x. The set includes the five $[HC]_0$ values of 1, 5, 10, 50 and 100 ppb. The

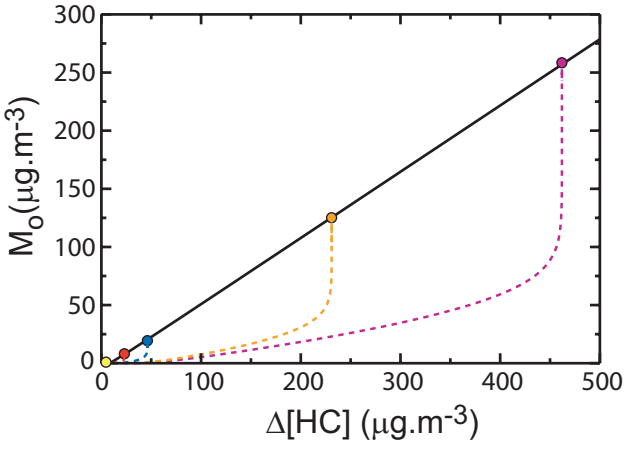

Fig. 8. Time-dependent and final growth curves simulated for the oxidation of 1-octene under 1 ppb of NO_x. Five simulations were carried out with various initial loadings of 1-octene. Each dashed line represents the evolution of M_o during a single simulation. Each circle represents $M_o^{\max}$ obtained for this simulation. The continuous line represents the final growth curve.

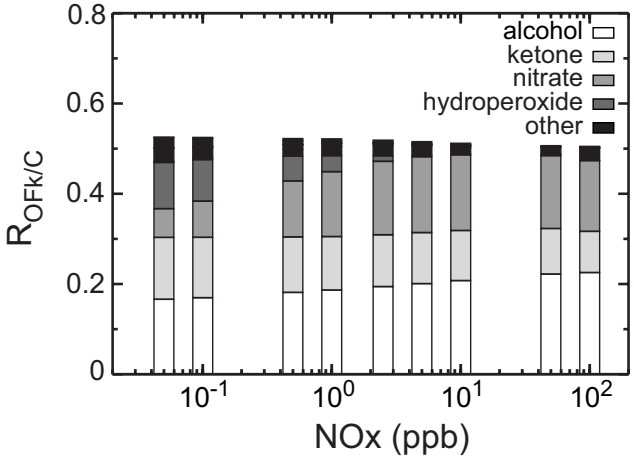

Fig. 9. Distribution of the ratio of organic functional group per particulate carbon ($R_{OFk/C}$) as a function of NO_x level for simulations carried out with an initial loading of 10 ppb of 1-octene.The distribution of ($R_{OFk/C}$)is plotted at the maximum aerosol yield.

final growth curve is also reported (as also shown Fig. 4a). The time-dependent growth curve does not overlap the final growth curve. This behaviour, characterised by a vertical section of the growth curve, is interpreted by Ng et al. (2006) as the result of SOA formation occurring after multiple oxidation steps. We showed in the previous section that SOA formation from octene oxidation is the result of species bearing at least 3 functional groups, formed by multiple oxidation steps. The behaviour observed in Fig. 8 therefore confirms the interpretation provided by Ng et al. (2006) to explain the shape of the curve.

5.3 SOA speciation sensitivity

The identities of secondary gaseous organics produced during gas-phase oxidation are a function of NO_x levels (e.g., Atkinson, 2000). NO_x level controls the fate of peroxy radical intermediates by changing the branching ratios in the radical photochemistry. Organic nitrate formation versus organic peroxide formation is thus directly affected by NO_x. NO_x is consequently suspected to influence SOA speciation, and therefore organic particulate matter ageing. At low NO_x, gaseous reactions with HO_2 may form peroxides (e.g., Atkinson, 2000). Gas/particle partitioning of hydroperoxides at low NO_x has been shown in both laboratory chamber experiments (Docherty et al., 2005; Tobias and Ziemann, 2001) and modelling studies (Bonn et al., 2004; Johnson et al., 2004, 2005) to represent a dominant fraction of SOA. Under high NO_x, gaseous reaction of RO_2 with NO produces organic nitrates among other products. Partitioning into nitrate moieties at high NO_x has been detected in experiments (e.g., Presto et al., 2005).

The distribution of the organic moieties ($R_{OFk/C}$) in the particulate phase at the maximum aerosol yield is shown in Fig. 9. Those values are plotted as a function of NO_x for the simulation carried out with 10 ppb of $[HC]_0$. The substitution degree of the carbon (i.e. $\sum_k R_{OFk/C}$) is found to be slightly sensitive to NO_x level and $[HC]_0$, with values raging around 40 to 50%. At all NO_x levels, the dominant moieties are found to be the alcohol ($15\% < R_{OH/C} < 25\%$) and the ketone ($R_{-CO-/C} < 13\%$). As expected at low NO_x, hydroperoxide moieties are a large fraction of SOA ($R_{-OOH/C}$=12%), while at high NO_x, nitrate moieties prevail ($R_{-ONO_2/C}$=18%).

6 Conclusions

An explicit model has been developed to explore (i) the potential of the products of multiple oxidation steps to play a role as SOA contributors and (ii) the evolution of the SOA/VOC/NO_x system. The sensitivity of the SOA/VOC/NO_x system has been studied for the oxidation of 1-octene under tropospheric relevant concentrations.

In this exploratory study, gaseous oxidation of octene is simulated to lead to SOA formation. Contributors to SOA formation are shown to be formed via multiple oxidation steps of the parent hydrocarbon. Time scales of a few days are indeed required to form those low vapour pressure products. This delay may explain why negligible or small SOA formation is observed in laboratory chamber experiments from the oxidation of relatively high volatile precursors.

The explicit approach captures the qualitative features observed during laboratory chamber experiments of the SOA/VOC/NO_x system:

– Y^{max} is found to be largely dependent on $[HC]_0$ at low $[HC]_0$ and tends to an asymptotic value when $[HC]_0$ tends to infinity.

– Y^{max} increases with NO_x at low NO_x and shows an opposite behaviour at high NO_x.

Maximum Y^{max} values are reached for a VOC(ppb)/NO_x(ppb) ratio of about 10. Simulated results lead to the conclusions that the dependence of Y^{max} with NO_x is here the result of (i) the relative contribution of oxidants, (ii) the gaseous oxidation rate and (iii) the gaseous radical chemistry. Furthermore the simulated temporal behaviour of SOA formation corroborates the interpretation provided by Ng et al. (2006) for SOA formation from multiple oxidation steps of the parent compound. The simulated speciation shows a large contribution of hydroperoxide moieties at low NO_x while at high NO_x, nitrate moieties prevail as expected.

As a result, such an explicit model can be used as a useful exploratory tool to (i) facilitate interpretations of SOA formation observed in laboratory chamber experiments, (ii) give some insights of SOA formation under relevant atmospheric conditions and (iii) examine the implications for the regional/global lifetimes of the SOA.

Acknowledgements. SM and JL-T wish to acknowledge support from DOE Grant No. DE-FG02-05ER63993. The National Center for Atmospheric Research is operated by the University Corporation for Atmospheric Research under support from the National Science Foundation.

Edited by: R. MacKenzie

References

Atkinson, R.: Atmospheric chemistry of VOCs and NO_x, Atmos. Environ., 34, 2063–2101, 2000.

Aumont, B., Madronich, S., Bey, I., and Tyndall, G. S.: Contribution of secondary VOC to the composition of aqueous atmospheric particles: a modelling approach, J. Atmos. Chem., 35, 59–75, 2000.

Aumont, B., Szopa, S., and Madronich, S.: Modelling the evolution of organic carbon during its gas-phase tropospheric oxidation: development of an explicit model based on a self generating approach, Atmos. Chem. Phys., 5, 2497–2517, 2005, http://www.atmos-chem-phys.net/5/2497/2005/.

Bey, I., Jacob, D., Yantosca, R. M., Logan, J. A., Field, B. D., Fiore, A. M., Li, Q., Liu, H., and Mickeley, L. J.: Global modeling of tropospheric chemistry with assimilated meteorology: model description and evaluation, J. Geophys. Res., 106, 23 073–23 096, 2001.

Bonn, B., von Kuhlmann, R., and Lawrence, M. G.: High contribution of biogenic hydroperoxides to secondary organic aerosol formation, Geophys. Res. Lett., 31, L10108, doi:10.1029/2003GL019172, 2004.

Brasseur, G. P., Hauglustaine, D. A., Walters, S., Rasch, P. J., Muller, J.-F., Granier, C., and Tie, X. X.: MOZART: a global chemical transport model for ozone and related chemical tracers, Part 1. Model description, J. Geophys. Res., 103, 28 265–28 289, 1998.

Calvert, J. G., Atkinson, R., Kerr, J. A., Madronich, S., Moortgat, G. K., Wallington, T. J., and Yarwood, G.: The mechanisms of atmospheric oxidation of the alkenes, Oxford University Press, London, 2000.

Camredon, M., and Aumont, B.: Assessment of vapor pressure estimation methods for secondary organic aerosol modeling, Atmos. Environ., 40, 2105–2116, 2006.

Carter, W. P. L.: Documentation of the SAPRC-99 chemical mechanism for the VOC reactivity assessment, Final report to the California Air Resources Board under contracts 92-329 and 95-308, Center of Environmental Research and Technology, Riverside, 2000.

Chung, S. H. and Seinfeld, J. H.: Global distribution and climate forcing of carbonaceous aerosols, J. Geophys. Res., 107(D19), 4407, doi:10.1029/2001JD001397, 2002.

Cocker, D. R., Flagan, R. C., and Seinfeld, J. H.: State-of-the-art chamber facility for studying atmospheric aerosol chemistry, Environ. Sci. Technol., 35, 2594–2601, 2001.

de Gouw, J. A., Middlebrook, A. M., Warneke, C., Goldan, P. D., Kuster, W. C., Roberts, J. M., Fehsenfeld, F. C., Worsnop, D. R., Canagaratna, M. R., Pszenny, A. A. P., Keene, W. C., Marchewka, M., Bertman, S. B., and Bates, T. S.: Budget of organic carbon in a polluted atmosphere: results from the New England air quality study in 2002, J. Geophys. Res., 110, D16305, doi:10.1029/2004JD005623, 2005.

Docherty, K. S., Wilbur Wu, P. J., Yong Bin Lim, P. J., and Ziemann, P. J.: Contributions of organic peroxides to secondary aerosol formed from reactions of monoterpenes with O_3, Environ. Sci. Technol., 39, 4049–4059, 2005.

Forstner, H. J. L., Flagan, R. C., and Seinfeld, J. H.: Molecular speciation of secondary organic aerosol from photooxidation of the higher alkenes: 1-octene and 1-decene, Atmos. Environ., 31, 1953–1964, 1997.

Gao, S., Ng, N. L., Keywood, M., Varutbangkul, V., Bahreini, R., Nenes, A., He, J., Yoo, K. Y., Beauchamps, J. L., Hodyss, R. P., Flagan, R., and Seinfeld, J. H.: Particle phase acidity and oligomer formation in secondary organic aerosol, Environ. Sci. Technol., 38, 6582–6589, 2004.

Gery, M., Whitten, G. Z., Killus, J., and Dodge, M.: A photochemical kinetics mechanism for urban and regional computer modeling, J. Geophys. Res., 94, 12 925–12 956, 1989.

Griffin, R. J., Cocker, D. R., Flagan, R. C., and Seinfeld, J. H.: Organic aerosol formation from the oxidation of biogenic hydrocarbons, J. Geophys. Res., 104, 3555–3567, 1999.

Hatakeyama, S., Izumi, K., Fukuyama, T., Akimoto, H., and Washida, N.: Reactions of OH with α-pinene and β-pinene in air: estimate of global CO production and atmospheric oxidation of terpenes, J. Geophys. Res., 96, 947–958, 1991.

Heald, C. L., Jacob, D. J., Park, R. J., Russell, L. M., Huebert, B. J., Seinfeld, J. H., Liao, H., and Weber, R. J.: A large organic aerosol source in the free troposphere missing from current models, Geophys. Res. Lett., 32, L18809, doi:10.1029/2005GL023831, 2005.

Hoffman, T., Odum, J. R., Bowman, F., Collins, D., Klockow, D., Flagan, R. C., and Seinfeld, J. H.: Formation of organic aerosols from the oxidation of biogenic hydrocarbons, J. Atmos. Chem.,

26, 189–222, 1997.

Hurley, M. D., Sokolov, O., Wallington, T. J., Takekawa, H., Karasawa, M., Klotz, B., Barnes, I. A. N., and Becker, K. H.: Organic aerosol formation during the atmospheric degradation of toluene, Environ. Sci. Technol., 35, 1358–1366, 2001.

Jacobson, M. C., Hansson, H. C., Noone K. J., and Charlson, R. J.: Organic atmospheric aerosols: review and state of the science, Rev. Geophys., 38, 267–294, 2000.

Jang, M., Czoschke, N. M., Lee, S., and Kamens, R. M.: Heterogeneous atmospheric organic aerosol production by inorganic acid-catalyzed particle-phase reactions, Science, 298, 814–817, 2002.

Jenkin, M. E., Saunders, S. M., Wagner, V., and Pilling, M. J.: Protocol for the development of the Master Chemical Mechanism, MCM v3 (Part B): tropospheric degradation of aromatic volatile organic compounds, Atmos. Chem. Phys., 3, 181–193, 2003, http://www.atmos-chem-phys.net/3/181/2003/.

Johnson, D., Jenkin, M. E., Wirtz, K., and Martin-Reviejo, M.: Simulating the formation of secondary organic aerosol from photooxidation of toluene, Environ. Chem., 1, 150–165, 2004.

Johnson, D., Jenkin, M. E., Wirtz, K. and Martin-Reviejo, M.: Simulating the formation of SOA from the photooxidation of aromatic hydrocarbons, Environ. Chem., 2, 35–48, 2005.

Johnson, D., Utembe, S. R., and Jenkin, M. E.: Simulating the detailed chemical composition of secondary organic aerosol formed on a regional scale during the TORCH 2003 campaign in the southern UK, Atmos. Chem. Phys., 6, 419–431, 2006, http://www.atmos-chem-phys.net/6/419/2006/.

Kalberer, M., Yu, J., Cocker, D. R., Flagan, R. C., and Seinfeld, J. H.: Aerosol formation in the cyclohexene-ozone system, Environ. Sci. Technol., 34, 4894–4901, 2000.

Kalberer, M., Paulsen, D., Sax, M., Steinbacher, M., Dommen, J., Prevot, A. S. H., Fisseha, R., Weingartner, E., Frankevich, V., Zenobi, R., and Baltensperger, U.: Identification of polymers as major components of atmospheric organic aerosols, Science, 303, 1659–1662, 2004.

Kanakidou, M., Tsigaridis, K., Dentener, F. J., and Crutzen, P. J.: Human-activity-enhanced formation of organic aerosols by biogenic hydrocarbon oxidation, J. Geophys. Res., 105, 9243–9254, 2000.

Kanakidou, M., Seinfeld, J. H., Pandis, S. N., Barnes, I., Dentener, F. J., Facchini, M. C., Van Dingenen, R., Ervens, B., Nenes, A., Nielsen, C. J., Swietlicki, E., Putaud, J. P., Balkanski, Y., Fuzzi, S., Horth, J., Moortgat, G. K., Winterhalter, R., Myhre, C. E. L., Tsigaridis, K., Vignati, E., Stephanou, E. G., and Wilson, J.: Organic aerosol and global climate modelling: a review, Atmos. Chem. Phys., 5, 1053–1123, 2005, http://www.atmos-chem-phys.net/5/1053/2005/.

Kroll, J. H. and Seinfeld, J. H.: Representation of secondary organic aerosol laboratory chamber data for the interpretation of mechanisms of particle growth, Environ. Sci. Technol., 39, 4159–4165, 2005.

Kroll, J. H., Ng, N. L., Murphy, S. M., Flagan, R. C., and Seinfeld, J. H.: Secondary organic aerosol formation from isoprene photooxidation, Environ. Sci. Technol., 40, 1869–1877, 2006.

Kroll, J. H., Chan, A. W. H., Ng, N. L., Flagan, R. C., and Seinfeld, J. H.: Reactions of semivolatile organics and their effects on secondary organic aerosol formation, Environ. Sci. Technol., 41, 3545–3550, 2007.

Madronich, S. and Calvert, J. G.: Permutation reactions of organic peroxy radicals in the troposphere, J. Geophys. Res., 95, 5697–5715, 1990.

Madronich, S. and Flocke, S.: The role of solar radiation in atmospheic chemistry, Handbook of environmental chemistry, Springer, New York, 1–26, 1998.

Martin-Riviejo, M. and Wirtz, K.: Is benzene a precursor for secondary organic aerosol?, Environ. Sci. Technol., 39, 1045–1054, 2005.

Molina, M. J., Ivanov, A. V., Trakhtenberg, S., and Molina, L. T.: Atmospheric evolution of organic aerosol, Geophys. Res. Lett., 31, L22104, doi:10.1029/2004GL020910, 2004.

Myrdal, P. B. and Yalkowsky, S. H.: Estimating pure component vapor pressures of complex organic molecules, Ind. Eng. Chem. Res., 36, 2494–2499, 1997.

Ng, N. L., Kroll, J. H., Keywood, M. D., Bahreini, R., Varutbangkul, V., Flagan, R. C., Seinfeld, J. H., Lee, A., and Goldstein, A. H.: Contribution of first- versus second-generation products to secondary organic aerosols formed in the oxidation of biogenic hydrocarbons, Environ. Sci. Technol., 40, 2283–2297, 2006.

Ng, N. L., Kroll, J. H., Chan, A. W. H., Chhabra, P. S., Flagan, R. C., and Seinfeld, J. H.: Secondary organic aerosol formation from m-xylene, toluene, and benzene, Atmos. Chem. Phys., 7, 3909–3922, 2007, http://www.atmos-chem-phys.net/7/3909/2007/.

Odum, J. R., Hoffmann, T., Bowman, F., Collins, D., Flagan, R. C., and Seinfeld, J. H.: Gas/particle partitioning and secondary aerosol yields, Environ. Sci. Technol., 30, 2580–2585, 1996.

Odum, J. R., Jungkamp, T. P. W., Griffin, R. J., Forstner, H. J. L., Flagan, R. C., and Seinfeld, J. H.: Aromatics, reformulated gasoline, and atmospheric organic aerosol formation, Environ. Sci. Technol., 31, 1890–1897, 1997.

Pandis, S. N., Paulson, S. E., Seinfeld, J. H., and Flagan, R. C.: Aerosol formation in the photooxidation of isoprene and α-pinene, Atmos. Environ., 25, 997–1008, 1991.

Pankow, J. F.: An absorption model of gas/particle partitioning of organic compounds in the atmosphere, Atmos. Environ., 28, 185–188, 1994a.

Pankow, J. F.: An absorption model of the gas/aerosol partioning involved in the formation of secondary organic aerosol, Atmos. Environ., 28, 189–193, 1994b.

Poisson, N., Kanakidou, M. A., and Crutzen, P. J.: Impact of non-methane hydrocarbons on 20 tropospheric chemistry and the oxidizing power of the global troposphere: 3-dimensional modelling results, J. Atmos. Chem., 36, 157–230, 2000.

Presto, A. A., Huff Hartz, K. E., and Donahue, N. M.: Secondary organic aerosol production from terpene ozonolysis. 2. Effect of NO_x concentration, Environ. Sci. Technol., 39, 7046–7054, 2005.

Puxbaum, H., Rendl, J., Allabashi, R., Otter, L., and Scholes, M. C.: Mass balance of atmospheric aerosol in a South-African subtropical savanna (Nylsvley, May 1997), J. Geophys. Res., 105, 20 697–20 706, 2000.

Reid, R. C., Prausnitz, J. M., and Polling, B. E.: The properties of gases and liquids, 4th edition, McGraw-Hill, Inc., New York, 1986.

Rogge, W. F., Mazurek, M. A., Hildemann, L. M., Cass, G. R., Simoneit, B. R. T.: Quantification of urban organic aerosols at a molecular level: identification, abundance and seasonal varia-

tion, Atmos. Environ., 27A, 1309–1330, 1993.

Saunders, S. M., Jenkin, M. E., Derwent, R. G., and Pilling, M. J.: Protocol for the development of the Master Chemical Mechanism, MCM v3 (Part A): tropospheric degradation of non-aromatic volatile organic compounds, Atmos. Chem. Phys., 3, 161–180, 2003, http://www.atmos-chem-phys.net/3/161/2003/.

Schell, B., Ackermann, I. J., Hass, H., Binkowski, F. S., and Ebel, A.: Modeling the formation of secondary organic aerosol within a comprehensive air quality model system, J. Geophys. Res., 106, 28 275–28 293, 2001.

Seinfeld, J. H. and Pankow, J. F.: Organic atmospheric particulate material, Annu. Rev. Phys. Chem., 54, 121–140, 2003.

Song, C., Na, K., and Cocker III, D. R.: Impact of the hydrocarbon to NO_x ratio on secondary organic aerosol formation, Environ. Sci. Technol., 39, 3143–3149, 2005.

Stephanou, E. G.: The decay of organic aerosols, Nature, 434, p. 31, 2005.

Stockwell, W. R., Kirchner, F., Kuhn, M., and Seefeld, S.: A new mechanism for regional atmospheric chemistry modeling, J. Geophys. Res., 102, 25 847–25 879, 1997.

Tobias, H. J. and Ziemann, P. J.: Kinetics of the gas-phase reactions of alcohols, aldehydes, carboxylic acids, and water with the C13 stabilized Criegee Intermediate formed from ozonolysis of 1-tetradecene, J. Phys. Chem. A, 105, 6129–6135, 2001.

Tolocka, M. P., Jang, M., Ginter, J. M., Cox, F. J., Kamens, R. M., and Johnston, M. V.: Formation of oligomers in secondary organic aerosol, Environ. Sci. Technol., 38, 1428–1434, 2004.

Tsigaridis, K. and Kanakidou, M.: Global modelling of secondary organic aerosol in the troposphere: a sensitivity analysis, Atmos. Chem. Phys., 3, 2879–2929, 2003, http://www.atmos-chem-phys.net/3/2879/2003/.

Turpin, B. J., Saxena, P., and Andrews, E.: Measuring and simulating particulate organics in the atmosphere: problems and prospects, Atmos. Environ., 34, 2983–3013, 2000.

Verwer, J. G.: Gauss-Seidel iteration for stiff ODEs from chemical kinetics, SIAM J. Sci. Comput., 15, 1243–1250, 1994.

Verwer, J. G., Blom, J. G., Van Loon, M., and Spee, E. J.: A comparison of stiff ODE solvers for atmospheric chemistry problems, Atmos. Environ., 30, 49–58, 1996.

Vesterinen, M., Lehtinen, K. E. J., Kulmala, M., and Laaksonen, A.: Effect of particle phase oligomer formation on aerosol growth, Atmos. Environ., 41, 1768–1776, 2007.

Volkamer, R., Jimenez, J. L., San Martini, F., Dzepina, K., Zhang, Q., Salcedo, D., Molina, L. T., Worsnop, D. R., and Molina, M. J.: Secondary organic aerosol formation from anthropogenic air pollution: rapid and higher than expected, Geophys. Res. Lett., 33, L17811, doi:10.1029/2006GL026899, 2006.

Wang, S.-C., Paulson, S. E., Grosjean, D., Flagan, R. C., and Seinfeld, J. H.: Aerosol formation and growth in atmospheric organic/NO_x systems-I. Outdoor smog chamber studies of C7- and C8-hydrocarbons, Atmos. Environ., 26A, 403–420, 1992.

Zhang, S.-H., Shaw, M., Seinfeld, J. H., and Flagan, R. C.: Photochemical aerosol formation from α-pinene and β-pinene, J. Geophys. Res., 97(D18), 20 717–20 729, 1992.